Broadband Decoupling at High magnetic Fields: Challenges and Solutions

Robin A. de Graaf
MRRC, Yale University, New Haven, CT, USA
robin.degraaf@yale.edu

Introduction

In any scalar-coupled spin-system the resonance lines are split into multiple lines of smaller intensity. *Decoupling* refers to a technique in which the multiple lines are merged back into one singlet resonance in order to (1) achieve improved signal-to-noise ratio and (2) achieve spectral simplification. In its simplest form decoupling can only achieve these goals for a single, on-resonance spectral line. *Broadband* decoupling therefore refers to the challenge of achieving these two goals for all resonances in the total spectral range. Since decoupling employs (high-powered) radiofrequency (RF) pulses during acquisition and since the spectral bandwidth increases at higher magnetic fields, the challenges for a successful implementation of broadband decoupling typically boil down to minimizing tissue heating (SAR), while optimizing signal recovery and artifact suppression. Here the principles of decoupling are described, together with the challenges and solution of broadband decoupling at high magnetic fields.

Principle of Decoupling

Decoupling is typically employed in heteronuclear experiments, for example carbon-13 detection with proton decoupling. While homonuclear decoupling is possible, it will not be discussed here as it is inherently narrow-banded. Since the carbon-13 spectral bandwidth is > 100 ppm (as opposed to < 5 ppm for protons), the proton-detected, carbon-decoupled experiment is technically the most challenging and will be used to discuss the principles of decoupling.

Consider a ^{13}C-labelled nucleus coupled to a proton, for example in [1-^{13}C]-formic acid (H^{13}COOH). The regular proton spectrum will be characterized by two resonances centered around 8.26 ppm ("the chemical shift") and separated by 218.6 Hz ("the scalar coupling constant J"). The single resonance line of regular formic acid is split into two resonances for the ^{13}C-labelled compound because the magnetic environment of the proton is dependent on the magnetic moment ("spin") of the attached ^{13}C nucleus. When the ^{13}C nucleus is in the β-state (anti-parallel to B_0) the frequency of the attached proton is J/2 higher than for regular formic acid, while the proton frequency is J/2 lower when the ^{13}C nucleus is in the α-state (parallel to B_0). Because the ^{1}H-^{13}C interaction is governed by the electrons in the chemical bond, the scalar coupling constant J is independent of the external magnetic field B_0. The appearance of two resonances can also be described more formally using the product operator formalism. Following excitation, the density matrix during acquisition is given by

$$\sigma(t) = H_x \cos \pi J_{CH} t + 2H_y C_z \sin \pi J_{CH} t \qquad [1]$$

where H and C are the proton and carbon-13 product operators along the specified axis (traditionally I and S or A and X are used) and J_{CH} is the heteronuclear scalar coupling

constant. Graphically, Eq. [1] describes the interchange between in-phase proton magnetization (H_x) along the x-axis of the rotating frame and anti-phase proton magnetization ($2H_yC_z$) along the y-axis (Fig. 1A).

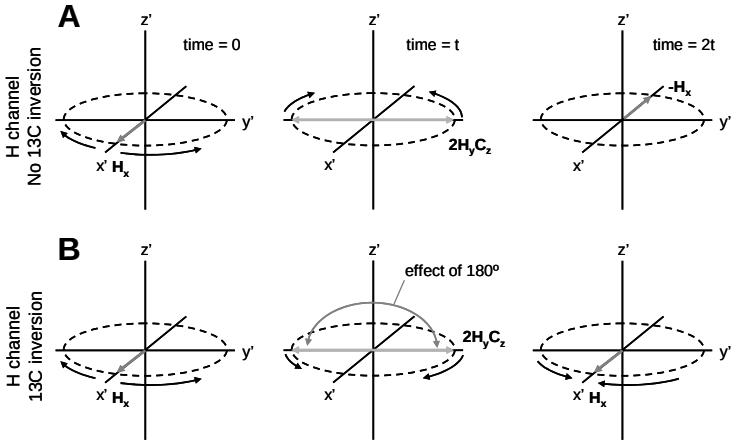

Fig. 1. Evolution of proton transverse magnetization in the (A) absence and (B) presence of a ^{13}C inversion pulse at time = t. Without an inversion pulse, the magnetization evolves as described by Eq. [1]. The inversion pulse inverts the ^{13}C spin-populations α and β, ultimately leading to refocusing of *proton* magnetization at time = 2t.

The key ingredient to decoupling is the utilization of spectrally-selective RF pulses. Fortunately in a ^{1}H-^{13}C heteronuclear system a regular (e.g. "square") RF pulse on the carbon-13 channel is automatically selective, since it does not directly perturb the attached protons. Following a delay t and a (selective) carbon-13 180º pulse the density matrix is given by

$$\sigma(t) = H_x \cos \pi J_{CH} t - 2H_y C_z \sin \pi J_{CH} t \qquad [2]$$

and at the end of an additional delay t, the density matrix is given by

$$\sigma(2t) = H_x \qquad [3]$$

In other words following a delay t, a selective ^{13}C 180 º pulse and an identical delay t the evolution due to scalar coupling has been refocused (Fig. 1B). Therefore, a decoupled ^{1}H NMR spectrum can be obtained when the proton acquisition points are timed to exactly correspond to multiples of 2t, i.e. the points of refocusing (Fig. 2B). For each acquisition point the effects of scalar coupling appear to be constant (i.e. frozen) and therefore only a single resonance will be observed at the proton frequency (note that proton chemical shifts are not refocused). While this simple experiment can theoretically work, a simple calculation will show that it is experimentally impractical. At 7.0 Tesla a reasonable proton spectral bandwidth is 4.0 kHz corresponding to a 250 us dwell-time (i.e. time between acquisition points). The length of the carbon-13 180º pulse can therefore be, at most 250 us, corresponding to a required B_1 strength of 2.0 kHz. Typically, proton signal would be acquired for ~250 ms corresponding to 1000 dwell-times and hence 1000 carbon-13 inversion pulses. Both the required peak power of 2.0 kHz, as well as the average power are unrealistic for human experiments. The peak power can simply not be met by RF amplifiers and coils, while the average power will lead to unacceptable tissue heating (specific absorption rate is proportional to B_{1av}^2 T). And unless the 180º pulses

are made much shorter than the dwell-time (and hence have much higher peak and average powers) an additional problem arises.

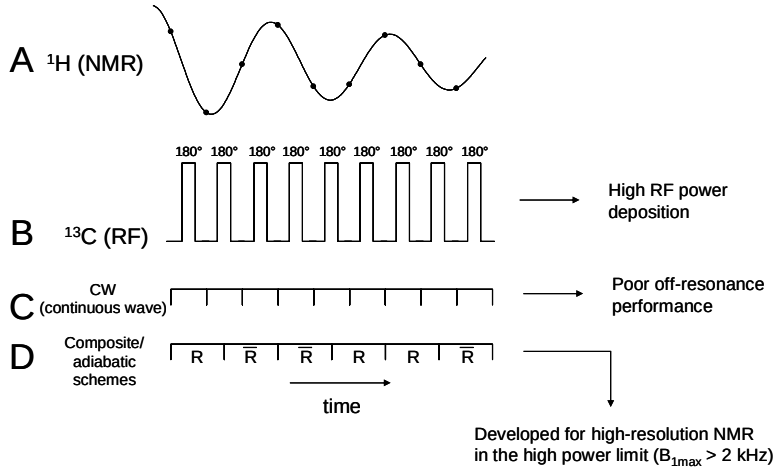

Fig. 2 Principle of broadband decoupling. (B) Perfect, infinitely short ^{13}C inversion pulses can be executed to give perfect refocusing of scalar evolution at each ^{1}H acquisition point (A), at the expense of unacceptable power deposition. (C) Stretching the inversion pulses to a single long pulse (CW) lowers the power deposition at the expense of poor off-resonance performance. (D) All successful decoupling method employs supercycles of pulses, in which R can be a series of composite or adiabatic pulses.

When the length of the 180º pulses is equal to the dwell-time, one essentially has a single, long RF pulse and the technique is often referred to as continuous wave (CW) decoupling. Unfortunately, the spectral bandwidth over which CW decoupling works is extremely limited (typically only a single on-resonance line can be decoupled), such that CW decoupling can not be considered as a broadband decoupling technique.

Broadband Inversion Pulses

While the principle of decoupling is relatively simple (see previous section), the challenge becomes on how to decouple wider spectral bandwidths without increasing the peak and average power and without increasing artifacts. The key to broadband decoupling is, obviously, the design of broadband inversion pulses. The first family of broadband inversion pulses that where implemented for broadband decoupling techniques are the so-called composite RF pulses. Composite pulses are composed of a number of RF pulses with different nutation angles and relative phases. While the overall rotation during a composite RF pulse is typically much larger than 180º, the final net nutation angle is close to 180º with some insensitivity towards frequency offsets and even towards B_1 inhomogeneity. The additional rotations are simply used to compensate the imperfection of a single 180º pulse by under- or over-rotating the magnetization where required. The two most successful composite pulses are $90^\circ_x 180^\circ_y 90^\circ_x$ and $90^\circ_x 180^\circ_{-x} 270^\circ_x$, forming the basis for MLEV (1) and WALTZ (2,3) decoupling. Fig. 3A shows the performance of a WALTZ inversion pulse relative to a conventional 180º pulse. Clearly, the off-resonance performance has greatly improved, as has the insensitivity towards B_1 inhomogeneity (not shown). While the individual composite RF pulses are already greatly improved, further improvements can be achieved by placing the composite pulses in so-called supercycles. For example, WALTZ-4 is composed of four successive segments $R_x R_x R_{-x} R_{-x}$ in which R_x is the original composite pulse. WALTZ-4 can be placed inside another supercycle, given rise to WALTZ-16, one of the most popular and commonly used decoupling sequence. The RF pulses further in the supercycle

compensate imperfections introduced to the earlier pulses. Composite pulses were initially designed based on visual representation of pulse rotations and are therefore ultimately limited by human ability to visualize complex rotations. Computational optimization of the nutation angle and relative phases of composite pulses has yielded several useful decoupling techniques (4-7).

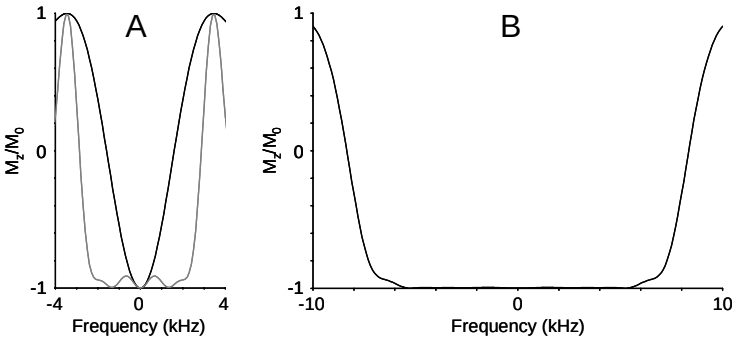

Fig. 3 Off-resonance performance of (A) 250 us square and 750 us WALTZ (gray) pulses and (B) a 3.0 ms AFPSTn, n=4 , R = 20 pulse. For all simulations B_1 = 2.0 kHz.

However, with the advent of ever higher magnetic fields even composite RF pulses can not achieve sufficient inversion bandwidths at reasonable power levels. As a result, the amplitude- and frequency-modulated adiabatic RF pulses were re-evaluated for use in broadband decoupling applications (8-10). In particular the adiabatic full passage (AFP) inversion pulses were investigated. Fig. 3B show the inversion profile of a hyperbolic secant AFP inversion pulse at the same peak power as the composite pulses of Fig. 3A. The inversion bandwidth is several times wider.

Broadband Decoupling

So far the off-resonance performance of inversion pulses has been discussed and while inversion pulses are a key ingredient in broadband decoupling it is not the only factor that determines the quality of decoupling. Because of power and SAR limitations, inversion pulses are typically stretched over several dwell-times. Even in the presence of perfect inversion pulses this will lead to artifacts called cycling sidebands (Fig. 4). In a perfect (high-power) experiment, signal refocusing according to Eq. [3] occurs at each data acquisition point (Fig. 4A). However, because the inversion pulse stretches over several acquisition points, scalar evolution is not perfectly refocused for the acquisition points before the end of the inversion pulse. As a result, the free induction decay (FID) will exhibit small modulations which, after Fourier transformation manifest themselves as (1) small cycling sidebands off the main decoupled peak and (2) a decrease in the mean decoupled peak intensity. The intensity, phase and frequency of the sidebands are a complicated function of the pulselength, the pulse shapes, the B_1 amplitude, the scalar coupling constant and the spin-system under investigation. While all of the effects can be experimentally assessed, Skinner and Bendall (11) have presented a theoretical product operator description of these phenomena, with which the performance of any decoupling sequence can be quantitatively described (12). Table I shows the performance of many common decoupling techniques as a function of the applied decoupling B_1 amplitude (12). It follows that for relatively low decoupling bandwidths WALTZ-16 and MLEV-16 offer superior performance. When very high decoupling bandwidths are required, for example for ^{13}C-decoupling at 11.74 T decoupling based on adiabatic RF pulses offer the only viable option. For intermediate decoupling bandwidths many options exist,

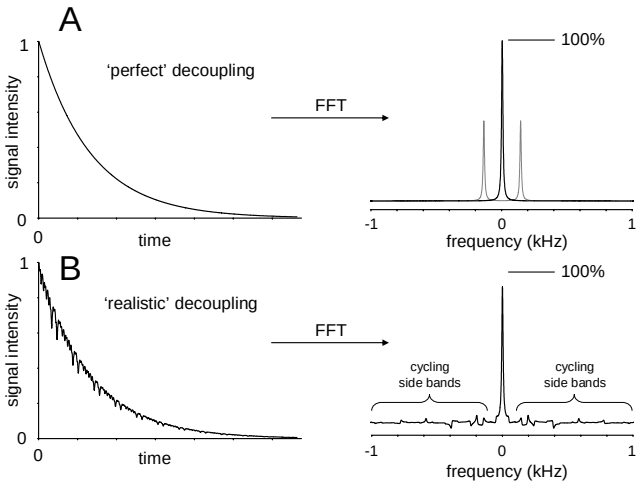

Fig. 4. Manifestation of decoupling sidebands. (A) During a perfect decoupling experiment (infinitely short square pulses) scalar evolution is refocused at each acquisition point and the signal decay is described by chemical shift evolution and T2 relaxation. In a two-spin-system, the NMR resonances will merge into a single resonance of double the intensity (100%). (B) With finite inversion pulses, scalar evolution is not refocused at each acquisition point leading to a small time-domain modulation which leads to decoupling sidebands in the spectrum and a lower decoupled resonance.

including decoupling based on optimized composite pulses. For most applications the required decoupling bandwidth ultimately determines the amount of RF power required. Therefore, for a given decoupling method, reducing the RF power is synonymous with reducing the spectral bandwidth. Proton observation with ^{13}C decoupling offers a unique window to RF power reduction, since the ^{13}C-labeled resonance are grouped from 10 to 60 ppm (amino acids) and from 90 ppm and up (glucose). Unlike composite decoupling, adiabatic decoupling can be made frequency-selective in that decoupling can be achieved between 10 and 60 ppm while simultaneously leaving resonances at other frequencies (e.g. glucose) unperturbed. This leads to an almost two-fold bandwidth reduction. Fig. 5 shows the high-quality proton-detected, carbon-decoupling NMR spectra that can be observed with this technique at 9.4 T.

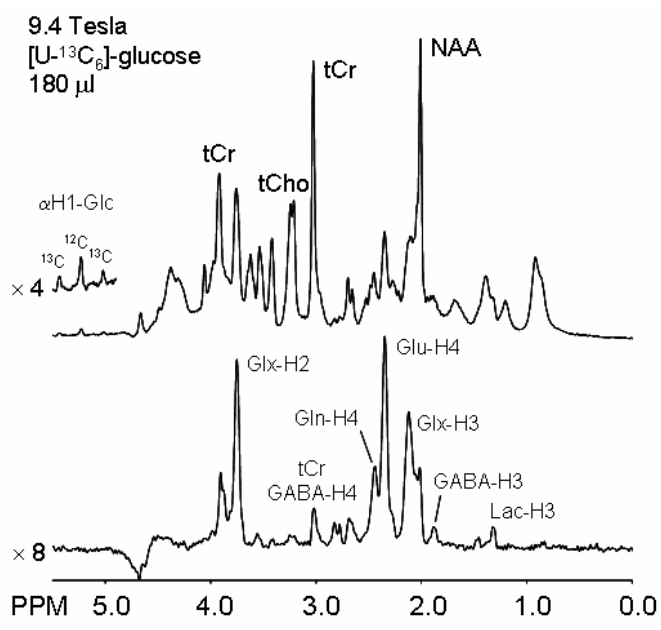

(A) ^{1}H and (B) ^{1}H-[^{13}C] edited NMR spectra acquired from rat brain (180 µL volume, *TR*/*TE* = 4000/8.5 ms, *NEX* = 512) at 9.4 T. Data acquisition began 2 h after the start of an intravenous [U-$^{13}C_6$]-glucose infusion. Selective adiabatic decoupling based on AFPST4 pulses (T = 1.5 ms, R = 10) was applied during the entire acquisition period (102 ms) with B_{2max} = 1600 Hz, corresponding to B_{2rms} = 1100 Hz. A frequency-selective ^{13}C inversion pulse was used for ^{13}C editing over the ^{13}C shift range of 10-60 ppm without perturbing the glucose-C1 resonances in the range 90-100 ppm. Therefore, the ^{1}H-[^{13}C] signals for glucose-C1 and the ^{1}H-[^{12}C]-signals for all species were edited out of spectrum (B).

Conclusions

Broadband decoupling is a RF-power intensive technique used to achieve improved signal-to-noise ratio and spectral simplification in heteronuclear NMR applications. Decoupling bandwidth and decoupling cycling sidebands ultimately determine the amount of RF power required. While one can not circumvent the minimum required RF power, one can choose the proper RF inversion pulses to achieve the widest bandwidths at the lowest decoupling sidebands. For certain specific applications, the use of selective decoupling can significantly reduce the RF power requirements.

References

1. Levitt MH, Freeman R. Composite pulse decoupling. J Magn Reson 1981;43:502-507.
2. Shaka AJ, Keeler J, Frenkiel T, Freeman R. An improved sequence for broadband decoupling: WALTZ-16. J Magn Reson 1983;52:335-338.
3. Shaka AJ, Keeler J, Freeman R. Evaluation of a new broadband decoupling sequence: WALTZ-16. J Magn Reson 1983;53:313-340.
4. Shaka AJ, Barker PB, Freeman R. Computer-optimized decoupling scheme for wideband applications and low-level operation. J Magn Reson 1985;64:547-552.
5. Fujiwara T, Nagayama K. Composite inversion pulses with frequency switching and their application to broadband decoupling. J Magn Reson 1988;77:53-63.
6. Fujiwara T, Nagayama K. Optimized frequency/phase-modulated broadband inversion pulses. J Magn Reson 1990;86:584-592.
7. Fujiwara T, Anai T, Kurihara N, Nagayama K. Frequency-switched composite pulses for decoupling carbon-13 spins over ultrabroad bandwidths. J Magn Reson A 1993;104:103-105.
8. Starcuk Z, Bartusek K, Starcuk Z. Heteronuclear broadband spin-flip decoupling with adiabatic pulses. J Magn Reson A 1994;107:24-31.
9. Bendall MR. Broadband and narrowband spin decoupling using adiabatic spin flips. J Magn Reson A 1995;112:126-129.
10. Kupce E, Freeman R. Adiabatic pulse for wideband inversion and broadband decoupling. J Magn Reson A 1995;115:273-276.
11. Skinner TE, Bendall MR. Exact product operator evolution of weakly coupled spin-12 I(m)S(n) systems during arbitrary RF irradiation of the I spins. J Magn Reson 1999;141(2):271-285.
12. de Graaf RA. Theoretical and experimental evaluation of broadband decoupling techniques for in vivo NMR spectroscopy. Magn Reson Med 2005;53:1297-1306.

Table 1: Relative decoupling bandwidths (BW_{90}/B_{2max}) as a function of B_{2max} or B_{2rms}

B_{2max} (kHz)	0.50	0.75	1.0	1.5
WALTZ-16	1.64	2.27	2.37	2.40
MLEV-16	1.74	2.05	2.18	2.21
F2	1.34	2.68	2.74	2.76
F3	0	3.21	4.13	4.17
FP2	1.38	2.12	2.17	2.20
FP3	1.22	2.61	2.92	3.30
GARP	0	0	1.65	4.96
PBAR	0.52	0.65	0.66	0.68
AFPSTn[a]	0	0.45	3.44	5.40
AFPTT[a]	0	1.96	2.72	3.55
B_{2rms} (kHz)	0.50	0.75	1.0	1.5
PBAR	0.66	0.67	0.68	0.68
AFPSTn[a]	1.48	3.36	4.36	7.53
AFPTT[a]	0	2.15	2.82	3.67

[a] The performance at different B_2 field strengths may correspond to AFP pulses with different R-values, pulse lengths or modulation functions.

Further details can be found in (12).